

Experimental Implementation of a Two-Stroke Quantum Heat Engine

Filipe V. Melo, Nahum Sá, Ithzak Roditi, Alexandre M. Souza, Ivan S. Oliveira, Roberto S. Sarthour
Centro Brasileiro de Pesquisas Físicas, Rio de Janeiro, Brazil

Gabriel T. Landi

*Instituto de Física da Universidade de São Paulo, São Paulo, Brazil and
 School of Physics, Trinity College Dublin, College Green, Dublin 2, Ireland*

(Dated: March 2022)

We put forth an experimental simulation of a stroboscopic two-stroke thermal engine in the IBMQ processor. The system consists of a quantum spin chain connected to two baths at their boundaries, prepared at different temperatures using the variational quantum thermalizer algorithm. The dynamics alternates between heat and work strokes, which can be separately designed using independent quantum circuits. The results show good agreement with theoretical predictions, showcasing IBMQ as a powerful tool to study thermodynamics in the quantum regime, as well as the implementation of variational quantum algorithms in real-world quantum computers. It also opens the possibility of simulating quantum heat transport across a broad range of chains geometries and interactions.

Energetics of quantum devices is an active topic of research [1], with many unique features. Quantum chains may present anomalous heat transport [2, 3], negative differential conductivity [4], and perfect rectification [5]. Often, the interaction energy between two systems is comparable to that of their individual parts [6–9], causing the local notion of energy, as belonging to individual systems, to break down. As a consequence, the separation between heat and work may become non-trivial, specially in the presence of quantum coherence. In the quantum domain, other resources also come into play: Quantum correlations, for example, can be consumed to make heat flow from cold to hot [10–12], similar to how electric energy is consumed to run a fridge. Finally, the invasive nature of quantum measurements makes all the above quantities extrinsic to the specific choice of measurement protocol [13–16].

The above arguments highlight the need for further experiments, able to assess the energetics of specific quantum devices. In this respect, quantum heat engines [17, 18] are particularly interesting, as they epitomize the fundamental questions of the field. Several experimental demonstrations of quantum heat engines have been put forth in recent years, including in trapped ions [19–22], nuclear magnetic resonance [23, 24], single electron boxes [25, 26] and nitrogen vacancy centers [27].

In this paper we provide an experimental simulation of a quantum heat engine in a superconducting device on the IBMQ network [28]. We focus on two-stroke engines, which alternate between heat and work strokes, in a generalization of the so-called SWAP engines [29–35]. The working fluid is a one-dimensional quantum chain, with both ends connected to thermal baths at different temperatures. Implementing thermal baths in quantum processors is notoriously difficult. In our setup this is overcome using a variational quantum thermalizer algorithm [36]. For the heat strokes, the sites are uncoupled

from each other, and allowed to interact with the baths at the boundaries. Conversely, in the work stroke the baths are uncoupled, and the qubits are allowed to interact with their nearest neighbors according to an arbitrary interaction [35]. The experiments are performed in the engine, refrigerator and accelerator configurations. We study both the transient dynamics, as well as the limit cycle.

The basic idea is depicted in fig. 1a. Our design, shown in fig. 1b, involves two separate and independent circuit implementations for the heat and work strokes. This has the unique advantage that it holds for any internal interaction during the work stroke. As a consequence, it can be implemented for any chain size and interaction that is programmable on the simulator.

The two-stroke heat engine we implement consists of a quantum chain with N uncoupled qubits, each with local Hamiltonian H_i , and prepared in an arbitrary global state ρ_S . The qubits can interact with their nearest neighbors, with a Hamiltonian $V_s = \sum_i V_{i,i+1}$ that can be turned on and off. In addition, one can also turn on and off an interaction between the qubits at the boundaries and two heat baths, modeled by identical and independently prepared qubits, with Hamiltonians H_x , and prepared in thermal states $\rho_x = e^{-H_x/T_x}/Z_x$, with $x \in \{C, H\}$, being C for cold and H for hot, Z_x is the partition function, and $T_C < T_H$ (we set $k_B = 1$).

The dynamics alternate between heat and work strokes. During the heat stroke, the internal interactions are turned off, while the boundary qubits interact with their respective baths C and H via Hamiltonians V_C and V_H . The system thus evolves for a period τ_q , under the action of a Hamiltonian, $H_q = \sum_i H_i + H_C + H_H + V_C + V_H$, and with an evolution characterized by the map

$$\tilde{\rho}_S = \mathcal{E}_q(\rho_s) = \text{Tr}_{CH}\{U_q(\rho_C \rho_S \rho_H) U_q^\dagger\}, \quad (1)$$

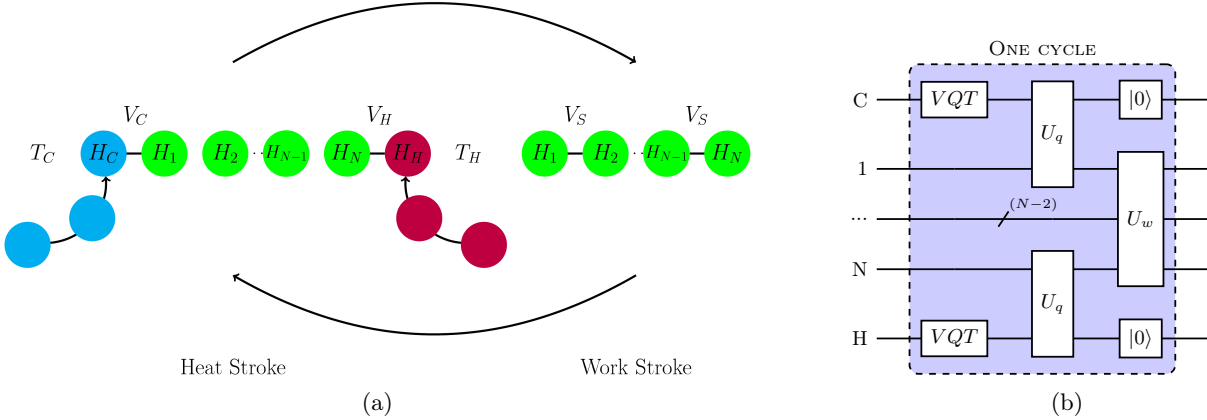


Figure 1: The quantum heat engine operates in two modes, as shown in (a): The heat stroke, and the work stroke. In the former, the internal interactions of the quantum chain are turned off and the system boundary qubits interact with a cold bath at temperature T_C and a hot bath at temperature T_H . In the latter, the baths are uncoupled and the chain qubits interact with their nearest neighbors. The strokes are operated in a cyclic way, and at each heat stroke a new bath is introduced, according to the collisional model. The experimental setup of a cycle, shown in (b), consists of $N + 2$ qubits (in our case $N = 2$). At the beginning, bath qubits C and H in the $|0\rangle$ state are processed with the variational quantum thermalizer (VQT) to prepare them in thermal states at temperatures T_C and T_H . A set of gates implement the heat stroke via a unitary U_q , when qubits 1 and N are measured. The experiment is repeated until the work stroke, which is implemented via an unitary U_w , after which all the chain's qubits are measured. The bath qubits are reset to $|0\rangle$ for the next cycle.

where $U_q = e^{-iH_q\tau_q}$. In the work stroke, the baths are disconnected from the chain and the internal interactions V_S are turned on, allowing energy to flow through the chain. The system evolves for a time τ_w under the action of the Hamiltonian $H_w = \sum_i H_i + V_S$, according to the map

$$\rho'_S = \mathcal{E}_w(\rho_S) = U_w \tilde{\rho}_S U_w^\dagger, \quad (2)$$

where $U_w = e^{-iH_w\tau_w}$. The execution of the two strokes in succession results in a cycle of duration $\tau = \tau_q + \tau_w$. Fig. 1b illustrates one such cycle. Crucially, for each new cycle the baths C and H are reset to the same temperatures T_C and T_H , as in a collisional model [37]. The machine thus follow a stroboscopic dynamics. Letting ρ_S^n denote the initial state of the n^{th} cycle, and $\tilde{\rho}_S^n$ the intermediate state between the strokes, the dynamics is given by

$$\tilde{\rho}_S^n = \mathcal{E}_q(\rho_S^n), \quad \rho_S^{n+1} = \mathcal{E}_w(\tilde{\rho}_S^n). \quad (3)$$

By splitting the dynamics in two strokes, we have reduced the problem to two independent simulation designs. For the work stroke, one need only design of U_w . Conversely, for the heat stroke, one must design both U_q and the thermal states of the reservoirs. The implementation of the latter is in practice quite difficult, and is overcome here using the algorithm put forth in [36], and detailed further below.

In order to track the energetics of the engine, we can measure the energy changes of the baths and the system during each cycle. In the heat stroke of the n^{th} cycle, we

define heat as the change in energy of the baths:

$$Q_x^n = -\text{Tr}\{H_x(\tilde{\rho}_S^n - \rho_S^n)\} \quad (4)$$

which are positive when energy enters the system. Notice that ρ_x is the same for all cycles, since the baths are reset. The heat Q_x^n is, in general, different from the change in energy of the system, as there may be a work cost associated to turning on/off the interactions $V_{C(H)}$. From global energy conservation, we find that [37]:

$$\begin{aligned} W_C^{\text{on/off}} &= Q_C^n + \text{Tr}\{H_1(\tilde{\rho}_S^n - \rho_S^n)\} = -\Delta V_C^n \\ W_H^{\text{on/off}} &= Q_H^n + \text{Tr}\{H_N(\tilde{\rho}_S^n - \rho_S^n)\} = -\Delta V_H^n \end{aligned} \quad (5)$$

with $\Delta V_x^n = \text{Tr}\{V_x(\tilde{\rho}_{CSH}^n - \rho_C \rho_S^n \rho_H)\}$.

This work term only vanishes when

$$[V_C, H_1 + H_C] = [V_H, H_N + H_H] = 0, \quad (6)$$

a condition known as *strict energy conservation* [35]. When this is satisfied, we can write

$$\begin{aligned} Q_C^n &= \text{Tr}\{H_1(\tilde{\rho}_S^n - \rho_S^n)\} \\ Q_H^n &= \text{Tr}\{H_N(\tilde{\rho}_S^n - \rho_S^n)\} \end{aligned} \quad (7)$$

meaning that all energy that leaves the bath enters the system and vice-versa. Thus, one can determine the change in energy during the heat stroke measuring only the state of the system chain.

During the work stroke, the interactions $V_S = \sum_i V_{i,i+1}$ are turned on so that energy is allowed to flow through the chain. The work cost associated to this is

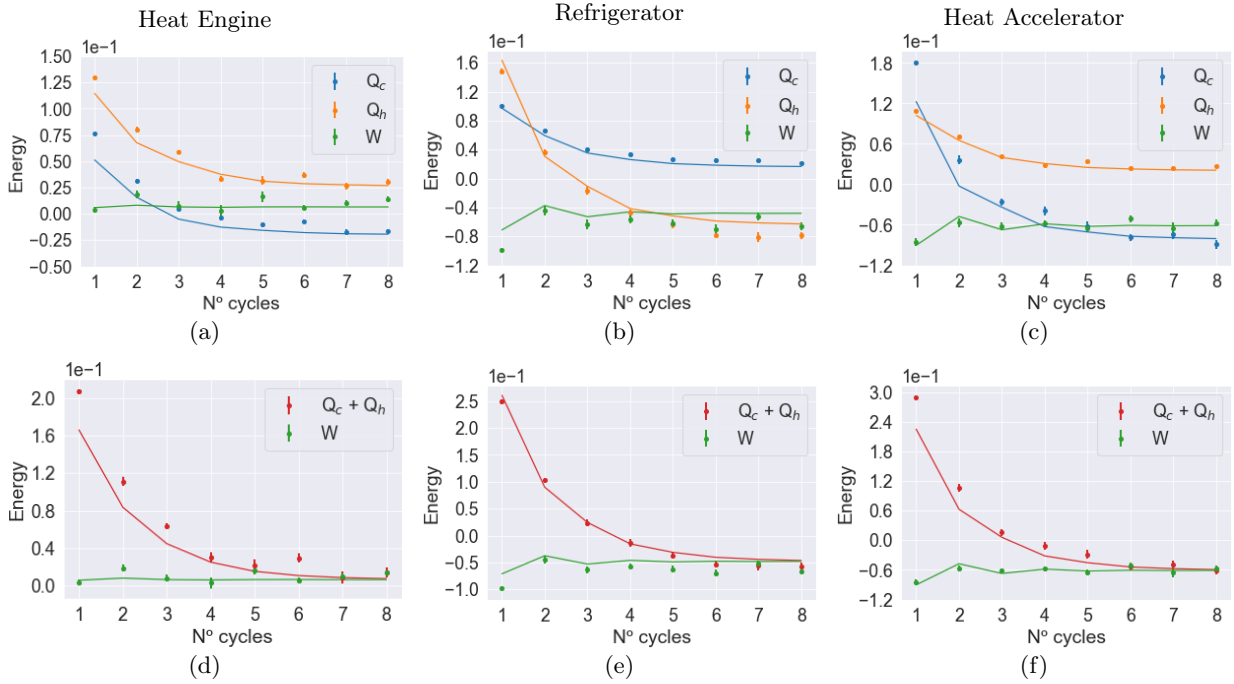


Figure 4: Results for the three different modes of operation. First column: heat engine ($\omega_1 = 0.75$, $\omega_2 = 1.0$, $g = 0.80$, $T_C = 0.40$, $T_H = 0.80$), second column: refrigerator ($\omega_1 = 0.50$, $\omega_2 = 2.0$, $g = 0.80$, $T_C = 1.0$, $T_H = 1.2$), third column: heat accelerator ($\omega_1 = 2.0$, $\omega_2 = 0.50$, $g = 0.80$, $T_C = 1.0$, $T_H = 1.2$). In all cases, both chain qubits were initialized in the ground state. Graphics (a)-(c) depict the dynamics of Q_C , Q_H and W during the machine operation; graphics (d)-(f) are a statement of the first law, showing that $Q_C + Q_H$ and W converge to the same value in the limit cycle. The circles represent experimental data, and the solid lines were obtained from a numerical simulation of the Trotter evolution. All results were obtained with 8192 shots (repetitions of the same circuit in order to build a statistics from the counts of $|0\rangle$ and $|1\rangle$). Each experiment was repeated 10 times, and the experimental points represent the mean of the results of the expectation values. The error bars were calculated from three times the standard deviation.

where \mathcal{Z}_β is the partition function. The details of the algorithm and its implementation can be seen in the supplementary material. At the end of the cycle, the bath qubits are reset to $|0\rangle$, so that the VQT may be applied again in the beginning of the next cycle, hence effectively generating a collisional model.

The interactions in the two strokes are simulated by finding a set of single- and two-qubit quantum gates \mathcal{U}_m and \mathcal{W}_m such that

$$U_q = \prod_{m=0}^M \mathcal{U}_m, \quad U_w = \prod_{m=0}^M \mathcal{W}_m \quad (20)$$

We implemented this using the *Operator Flow* module from the open-source framework *Qiskit* by IBM [38]. The circuits found for each stroke are illustrated in fig. 2.

We used the *ibm_lagos* (v1.0.8) processor, whose topology is shown in fig. 3. It allows the application of arbitrary single qubit rotations, as well as CNOT gates between connected qubits, and also reset operations. The average error associated with the CNOT gates and the readout is around 0.8% and 1%, respectively. The simulation must be planned taking into account the connectivity of the device, since applying CNOT gates to un-

connected qubits requires SWAP operations, which are very costly [28] and further complicate the implementation. In our problem, the interactions are all between neighboring qubits, thus, a good choice of layout is that shown in fig. 3.

The experiments were carried out for three different modes of operation of the machine: heat engine, refrigerator and heat accelerator. They are determined by the values of the frequencies ω_1 and ω_2 , and the temperatures T_C and T_H of the baths [34, 37]. These modes can be observed when the machine reaches the limit cycle. In the interval $T_C/T_H \leq \omega_1/\omega_2 \leq 1$, it operates as a heat engine, withdrawing heat from the hot bath ($Q_H > 0$), expelling some of it in the cold bath ($Q_C < 0$) and producing some useful work ($W > 0$). When $\omega_1/\omega_2 < T_C/T_H$, it works as a refrigerator, consuming work ($W < 0$) in order to extract heat from the cold bath and transfer it to the hot bath ($Q_C > 0$, $Q_H < 0$). When $\omega_1/\omega_2 > 1$, the machine operates as a heat accelerator, as it consumes work ($W < 0$) to accelerate the process of transferring heat from the hot to the cold bath ($Q_H > 0$, $Q_C < 0$).

The results are shown in fig. 4. The columns contain the results for each mode of operation. For comparison purposes, a numerical simulation of the Trotter evolu-

tion was performed, represented by the solid lines in the graphics. Graphics (a)-(c) shows the dynamics of the energetic flux during the cycles. As expected, the heat engine (a) and accelerator (c) show positive Q_H and negative Q_C in the limit cycle, whereas the refrigerator (b) presents the opposite behavior. During the work stroke, in the limit cycle, the heat engine produced work, as denoted by $W > 0$, and the refrigerator and heat accelerator both consumed work in order to operate, as denoted by $W < 0$. Graphics (d)-(f) shows that the system obeys the first law, as stated in eq. (13): in the limit cycle, the sum of the heats $Q_C + Q_H$ and the work W converge to the same quantity.

In summary, we experimentally demonstrated the use of the IBMQ processor as a tool to simulate quantum heat engines, with full access to the energetics of the system. Thermal reservoirs are particularly difficult to implement, which we overcame using a variational algorithm at each cycle, effectively implementing a collisional model. This allowed us to access both the limit cycle, as well as the transient regime, offering unique insights into the relaxation process. Our approach cleanly separates the heat and work strokes, and thus can be readily generalized to any other type of heat engines. This means either chains with multiple qubits, or more complicated interactions, opening up the prospect of simulating quantum heat engines and quantum transport in various many-body systems.

Acknowledgments. This study was financed in part by the Coordenação de Aperfeiçoamento de Pessoal de Nível Superior - Brasil (CAPES) - Finance Code 001, the Brazilian National Institute of Science and Technology for Quantum Information (INCT-IQ) Grant No. 465469/2014-0, the National Council for Scientific and Technological Development (CNPq), and the Carlos Chagas Filho Foundation for Research Support of Rio de Janeiro State (FAPERJ). GTL acknowledges the financial support of the São Paulo Funding Agency FAPESP (Grant No. 2019/14072-0), and CNPq (Grant No. INCT-IQ 246569/2014-0). IR also acknowledges CNPq (Grant No. 311876/2021-8). ISO acknowledges support from FAPERJ (Grant No. 202.518/2019). AMS acknowledges support from FAPERJ (Grant No. 203.166/2017).

[1] A. Auffèves, (2021), [arXiv:2111.09241v2 \[quant-ph\]](https://arxiv.org/abs/2111.09241v2).

[2] B. Bertini, F. Heidrich-Meisner, C. Karrasch, T. Prosen, R. Steinigeweg, and M. Žnidarič, *Reviews of Modern Physics* **93** (2021), [10.1103/revmodphys.93.025003](https://doi.org/10.1103/revmodphys.93.025003).

[3] G. T. Landi, D. Poletti, and G. Schaller, (2021), [arXiv:2104.14350v2 \[quant-ph\]](https://arxiv.org/abs/2104.14350v2).

[4] J. J. Mendoza-Arenas, T. Grujic, D. Jaksch, and S. R. Clark, *Physical Review B* **87** (2013), [10.1103/physrevb.87.235130](https://doi.org/10.1103/physrevb.87.235130).

[5] V. Balachandran, G. Benenti, E. Pereira, G. Casati, and D. Poletti, *Physical Review Letters* **120** (2018), [10.1103/physrevlett.120.200603](https://doi.org/10.1103/physrevlett.120.200603).

[6] C. Jarzynski, *Phys. Rev. X* **7**, 011008 (2017).

[7] M. Perarnau-Llobet, H. Wilming, A. Riera, R. Gallego, and J. Eisert, *Phys. Rev. Lett.* **120**, 120602 (2018).

[8] P. Strasberg, *Phys. Rev. Lett.* **123**, 180604 (2019).

[9] P. Talkner and P. Hänggi, *Rev. Mod. Phys.* **92**, 041002 (2020).

[10] M. H. Partovi, *Phys. Rev. E* **77**, 021110 (2008).

[11] D. Jennings and T. Rudolph, *Phys. Rev. E* **81**, 061130 (2010).

[12] K. Micadei, J. P. S. Peterson, A. M. Souza, R. S. Sarthour, I. S. Oliveira, G. T. Landi, T. B. Batalhão, R. M. Serra, and E. Lutz, *Nature Communications* **10**, 2456 (2019), [1711.03323](https://doi.org/10.1038/s41567-019-0532-3).

[13] M. Perarnau-Llobet, E. Bäumer, K. V. Hovhannisyan, M. Huber, and A. Acin, *Phys. Rev. Lett.* **118**, 070601 (2017).

[14] K. Micadei, G. T. Landi, and E. Lutz, *Phys. Rev. Lett.* **124**, 090602 (2020).

[15] A. Levy and M. Lostaglio, *PRX Quantum* **1**, 010309 (2020).

[16] K. Micadei, J. P. S. Peterson, A. M. Souza, R. S. Sarthour, I. S. Oliveira, G. T. Landi, R. M. Serra, and E. Lutz, *Phys. Rev. Lett.* **127**, 180603 (2021).

[17] R. Kosloff and A. Levy, *Annual Review of Physical Chemistry* **65**, 365 (2014).

[18] M. T. Mitchison, *Contemporary Physics* **60**, 164 (2019).

[19] J. Roßnagel, S. T. Dawkins, K. N. Tolazzi, O. Abah, E. Lutz, F. Schmidt-Kaler, and K. Singer, *Science* **352**, 325 (2016).

[20] D. von Lindenfels, O. Gräß, C. Schmiegelow, V. Kaushal, J. Schulz, M. T. Mitchison, J. Goold, F. Schmidt-Kaler, and U. Poschinger, *Physical Review Letters* **123** (2019), [10.1103/physrevlett.123.080602](https://doi.org/10.1103/physrevlett.123.080602).

[21] G. Maslennikov, S. Ding, R. Hablützel, J. Gan, A. Roulet, S. Nimmrichter, J. Dai, V. Scarani, and D. Matsukevich, *Nature Communications* **10** (2019), [10.1038/s41467-018-08090-0](https://doi.org/10.1038/s41467-018-08090-0).

[22] N. V. Horne, D. Yum, T. Dutta, P. Hänggi, J. Gong, D. Poletti, and M. Mukherjee, *npj Quantum Information* **6** (2020), [10.1038/s41534-020-0264-6](https://doi.org/10.1038/s41534-020-0264-6).

[23] J. P. Peterson, T. B. Batalhão, M. Herrera, A. M. Souza, R. S. Sarthour, I. S. Oliveira, and R. M. Serra, *Physical Review Letters* **123** (2019), [10.1103/physrevlett.123.240601](https://doi.org/10.1103/physrevlett.123.240601).

[24] T. Denzler, J. F. G. Santos, E. Lutz, and R. Serra, (2021), [arXiv:2104.13427v1 \[quant-ph\]](https://arxiv.org/abs/2104.13427v1).

[25] J. V. Koski, V. F. Maisi, J. P. Pekola, and D. V. Averin, *Proceedings of the National Academy of Sciences* **111**, 13786 (2014).

[26] J. Koski, A. Kutvonen, I. Khaymovich, T. Ala-Nissila, and J. Pekola, *Physical Review Letters* **115** (2015), [10.1103/physrevlett.115.260602](https://doi.org/10.1103/physrevlett.115.260602).

[27] J. Klatzow, J. N. Becker, P. M. Ledingham, C. Weinzel, K. T. Kaczmarek, D. J. Saunders, J. Nunn, I. A. Walmley, R. Uzdin, and E. Poem, *Physical Review Letters* **122** (2019), [10.1103/physrevlett.122.110601](https://doi.org/10.1103/physrevlett.122.110601).

[28] “Ibm quantum, <https://quantum-computing.ibm.com/>,” (2021).

[29] V. Scarani, M. Ziman, P. Štelmachovič, N. Gisin, and V. Bužek, *Physical Review Letters* **88** (2002), [10.1103/physrevlett.88.097905](https://doi.org/10.1103/physrevlett.88.097905).

- [30] H. T. Quan, Y. xi Liu, C. P. Sun, and F. Nori, *Physical Review E* **76** (2007), 10.1103/physreve.76.031105.
- [31] A. E. Allahverdyan, K. Hovhannisyan, and G. Mahler, *Physical Review E* **81** (2010), 10.1103/physreve.81.051129.
- [32] R. Uzdin and R. Kosloff, *New Journal of Physics* **16**, 095003 (2014).
- [33] M. Campisi, *Journal of Physics A: Mathematical and Theoretical* **47**, 245001 (2014).
- [34] M. Campisi, J. Pekola, and R. Fazio, *New Journal of Physics* **17**, 035012 (2015).
- [35] O. A. D. Molitor and G. T. Landi, *Physical Review A* **102** (2020), 10.1103/physreva.102.042217.
- [36] G. Verdon, J. Marks, S. Nanda, S. Leichenauer, and J. Hidary, “Quantum hamiltonian-based models and the variational quantum thermalizer algorithm,” (2019), [arXiv:1910.02071 \[quant-ph\]](https://arxiv.org/abs/1910.02071).
- [37] G. De Chiara, G. Landi, A. Hewgill, B. Reid, A. Ferraro, A. J. Roncaglia, and M. Antezza, *New Journal of Physics* **20**, 113024 (2018).
- [38] “Qiskit: An open-source framework for quantum computing,” (2019).
- [39] M. A. Nielsen and I. Chuang, “Quantum computation and quantum information,” (2002).
- [40] V. Bergholm, J. Izaac, M. Schuld, C. Gogolin, M. S. Alam, S. Ahmed, J. M. Arrazola, C. Blank, A. Delgado, S. Jahangiri, K. McKiernan, J. J. Meyer, Z. Niu, A. Száva, and N. Killoran, “Pennylane: Automatic differentiation of hybrid quantum-classical computations,” (2020), [arXiv:1811.04968 \[quant-ph\]](https://arxiv.org/abs/1811.04968).
- [41] M. J. Powell, in *Advances in optimization and numerical analysis* (Springer, 1994) pp. 51–67.
- [42] M. J. Powell, *Acta numerica* **7**, 287 (1998).

Supplementary Material

Variational Quantum Thermalizer

Here we describe the use of the *variational quantum thermalizer* (VQT), which belongs to a class of variational algorithms called *quantum-Hamiltonian based models* (QHBM), introduced by Verdon et. al [36]. The VQT algorithm was implemented in this work to simulate the thermal states of the bath qubits. Given a Hamiltonian H and a target inverse temperature $\beta = 1/T$, the goal of the VQT is to generate the best approximation to the thermal state:

$$\rho_\beta = \frac{1}{Z_\beta} e^{-\beta H}, \quad Z_\beta = \text{Tr}(e^{-\beta H}) \quad (21)$$

where Z_β is the partition function. We begin with a density matrix ρ_θ , defined by a set of pure states $\{|\psi_i\rangle\}$, that constitutes a basis on a Hilbert space of dimension d , and a parameter vector θ . Being $\{p_i(\theta_i)\}$ the probability distribution corresponding to the i -th basis state, such a matrix can be written as

$$\rho_\theta = \sum_{i=1}^d p_i(\theta_i) |\psi_i\rangle\langle\psi_i|. \quad (22)$$

We sample from this distribution a pure state $|\psi_i\rangle$, pass it through a parameterized quantum circuit $U(\phi)$, and measure the mean energy $\langle H \rangle_i = \langle \psi_i | U(\phi) H U^\dagger(\phi) | \psi_i \rangle$. Repeating this process many times for the set $\{|\psi_i\rangle\}$ and averaging the obtained $\langle H \rangle_i$ will give the mean energy $\langle H \rangle_{\theta\phi}$ with respect to $\rho_{\theta\phi} = U(\phi)\rho_\theta U^\dagger(\phi)$:

$$\langle H \rangle_{\theta\phi} = \sum_{i=1}^d p_i(\theta_i) \langle H \rangle_i. \quad (23)$$

As in any variational algorithm, in order to find the optimal parameters $\{\theta', \phi'\}$ that solve the problem, we must minimize a *loss function*, which here can be obtained from (23) and the von Neumann entropy $S(\rho_{\theta\phi})$. This would require two measurements, but we take advantage from the fact that the entropy is invariant under unitary transformations on the density matrix. Then, the loss function is:

$$\mathcal{L}(\theta, \phi) = \beta \langle H \rangle_{\theta\phi} - S(\rho_\theta), \quad (24)$$

which is minimized when $\rho_{\theta\phi}$ is equal to the required thermal state.

If ρ_θ is a factorized state composed of N subsystems $\rho_i(\theta_i)$:

$$\rho_\theta = \bigotimes_{i=1}^N \rho_i(\theta_i), \quad (25)$$

the number of $\{\theta\}$ parameters scales linearly with N , and the dimension of each subset $\{\theta_i\}$ is dependent only on

the internal structure of its related subsystem. Moreover, in this factorised form the entropy $S(\rho_\theta)$ is easier to calculate, as it is given by the sum of the entropy values for each subsystem:

$$S(\rho_\theta) = \sum_{i=1}^N S(\rho_i(\theta_i)). \quad (26)$$

The implemented ansatz is shown in fig. 5. We choose this particular ansatz because it can approximate any 1 qubit unitary, thus it doesn't depend on the Hamiltonian to be diagonal in the computational basis [39]. It also takes into account the set of gates accessible to the IBMQ device [28]. Other configurations were also tried, including rotations around other axes, but they did not show optimal results, and some demanded too many iterations of the VQT to converge. In order to implement the VQT in the experiment, we used the open-source Python libraries *Pennylane* by Xanadu [40] and *Qiskit* by IBM [38]. The classical optimization method chosen was the *Constrained Optimization BY Linear Approximation* (COBYLA) [41, 42], a gradient-free optimizer, which is a good choice as it reduces the number of circuit measurements.

When running the algorithm on a quantum computer, it is important that it is done in the corresponding qubits that will be used as baths, as in this case the VQT finds optimal parameters that consider the device noise associated to those qubits during the learning process. In general, it took less than 20 iterations for the algorithm to converge.

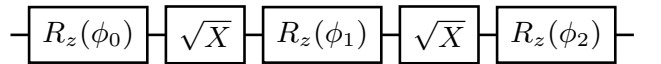


Figure 5: The chosen ansatz consists of three R_z rotations interspersed by square root of NOT gates. Each rotation has a different ϕ parameter, which are to be optimized during the VQT implementation.

Quantum Simulation

The quantum simulation step of the experiment involves finding a set of quantum gates in the IBMQ computer that can simulate the action of the Hamiltonians of each qubit. For the Hamiltonians H_C , H_H , H_1 and H_2 , the process involves a set of single qubit gates. To perform the interactions $V_{j,k}$, two qubit gates are necessary, taking into account the architecture of the processor. This task can be easily performed by implementing the *Operator Flow* module from *Qiskit* library, and the circuits found for each stroke are illustrated in fig. 6.

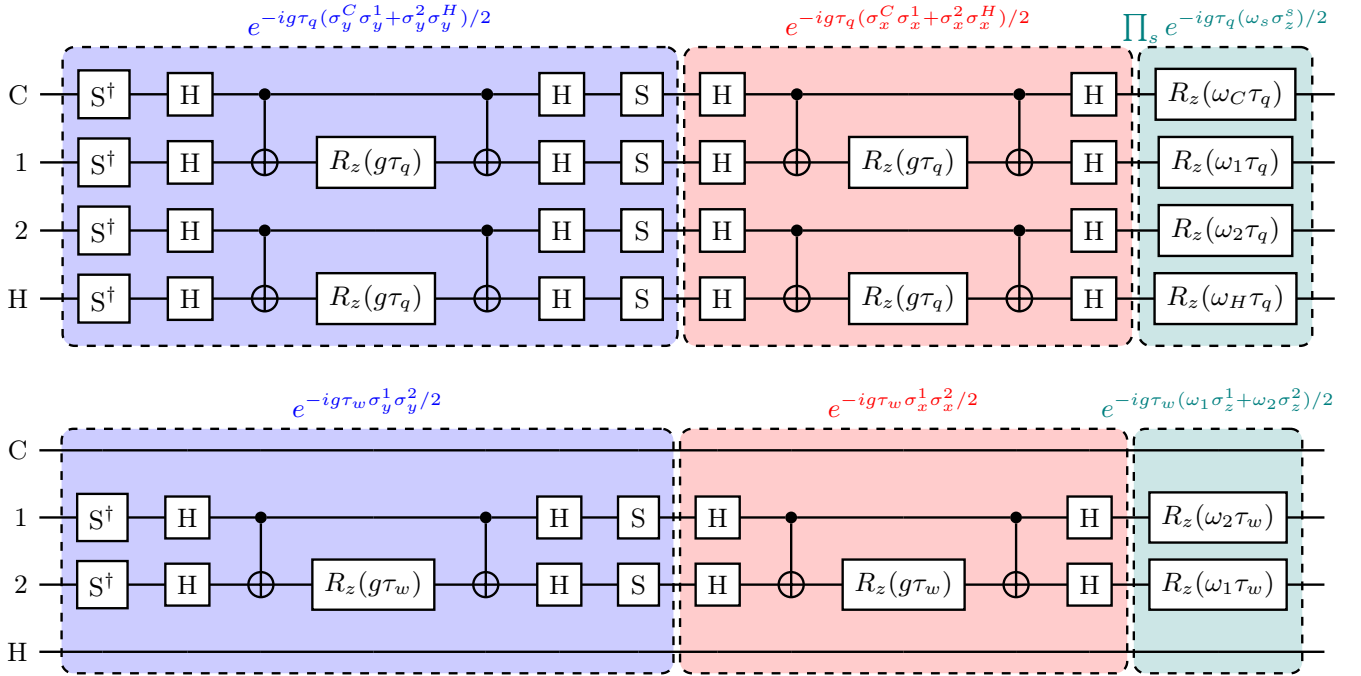


Figure 6: Quantum circuits for the simulation of the heat (above) and work (below) strokes. S and H represent phase and Hadamard gates, respectively, and $R_z(\theta)$ are rotations of an angle θ around the z -axis. The product on the green part of the first circuit is performed on the set $s = \{1, 2, C, H\}$.

Using the fact that $\sigma_+^i \sigma_-^j + \sigma_-^i \sigma_+^j = (\sigma_x^i \sigma_x^j + \sigma_y^i \sigma_y^j)/2$, the hamiltonian H_q for the heat stroke is written as:

$$\begin{aligned}
H_q &= H_1 + H_2 + H_C + H_H + V_{1,C} + V_{2,H} \\
&= \frac{\omega_1}{2} \sigma_z^1 + \frac{\omega_2}{2} \sigma_z^2 + \frac{\omega_C}{2} \sigma_z^C + \frac{\omega_H}{2} \sigma_z^H \\
&\quad + \frac{g}{2} (\sigma_x^1 \sigma_x^C + \sigma_y^1 \sigma_y^C) + \frac{g}{2} (\sigma_x^2 \sigma_x^H + \sigma_y^2 \sigma_y^H),
\end{aligned} \tag{27}$$

and H_w for the work stroke as:

$$\begin{aligned} H_w &= H_1 + H_2 + V_{1,2} \\ &= \frac{\omega_1}{2} \sigma_z^1 + \frac{\omega_2}{2} \sigma_z^2 + g(\sigma_+^1 \sigma_-^2 + \sigma_-^1 \sigma_+^2) \end{aligned} \quad (28)$$

Using the fact that $[\sigma_i \otimes \sigma_i, \sigma_j \otimes \sigma_j] = 0$ for $i, j \in x, y, z$, the resultant evolution operator U_q for the heat stroke may be conveniently written as

$$U_q = e^{-ig\tau_q(\sigma_y^C\sigma_y^1+\sigma_y^2\sigma_y^H)/2} \times \\ e^{-ig\tau_q(\sigma_x^C\sigma_x^1+\sigma_x^2\sigma_x^H)/2} \times \\ e^{-ig(\omega_1\sigma_z^1+\omega_2\sigma_z^2+\omega_C\sigma_z^C+\omega_H\sigma_z^H)/2} \quad (29)$$

and U_w for the work stroke as

$$U_w = e^{-ig\tau_w(\sigma_y^C\sigma_y^1+\sigma_y^2\sigma_y^H)/2} \times \\ e^{-ig\tau_w(\sigma_x^C\sigma_x^1+\sigma_x^2\sigma_x^H)/2} \times \\ e^{-ig(\omega_1\sigma_z^1+\omega_2\sigma_z^2)/2} \quad (30)$$

The set of gates that simulates the action of each part eq. (29) and eq. (30) are identified in fig. 6.

Measurement

In the IBM quantum computer, the measurements are performed in the σ_z -basis. Therefore, for a qubit in an arbitrary state $|\psi\rangle$ the expectation values $\langle\sigma_z^i\rangle_n$ can be directly calculated from the probabilities $p_0 = |\langle 0|\psi\rangle|^2$ and $p_1 = |\langle 1|\psi\rangle|^2$, which are provided at the end of the processes, since $\langle\sigma_z\rangle_i^n = p_0 - p_1$. These measurements are performed after the process is run many times, each run called a *shot*. The probabilities p_0 and p_1 can be obtained by dividing the number of times the system was found in the states $|0\rangle$ and $|1\rangle$, for each qubit, by the number of shots.